



# Thermal hazard analysis and thermokinetic calculation of 1,3-dimethylimidazolium nitrate via TG and VSP2

Bin Zhang<sup>1</sup> · Shang-Hao Liu<sup>1</sup> · Jen-Hao Chi<sup>2</sup>

Received: 16 April 2018 / Accepted: 12 July 2018 / Published online: 24 July 2018  
© Akadémiai Kiadó, Budapest, Hungary 2018

## Abstract

In this study, the thermal stability and thermokinetic parameters of 1,3-dimethylimidazolium nitrate ([Mmim]NO<sub>3</sub>) were investigated by thermogravimetric analysis under non-isothermal conditions in a nitrogen atmosphere. The results showed that [Mmim]NO<sub>3</sub> exhibited three decomposition stages from 93.3 to 350.0 °C, and the onset temperature of [Mmim]NO<sub>3</sub> was obtained at approximately 161.0–182.0 °C under five heating rates. The apparent activation energy was 119.0–124.0 kJ mol<sup>-1</sup>, as calculated by different well-known equations, and the pre-exponential factor was  $3.6 \times 10^{12} \text{ min}^{-1}$ . The reaction mechanism of [Mmim]NO<sub>3</sub> was carried out with the reaction order  $n = 1.0$ , and the decomposition mechanism function was further obtained. Moreover, vent sizing package 2 was employed to acquire the maximum self-heating rate (39,828.0 °C min<sup>-1</sup>) and pressure rise rate (73,331.0 psig min<sup>-1</sup>) for simulating cooling system failure in a practical process. The findings indicated that [Mmim]NO<sub>3</sub> showed the possibility of a runaway reaction, leading to a potential thermal hazard. The approach of these results is vital for obtaining inherently safer process information for [Mmim]NO<sub>3</sub> during production, storage, and transportation.

**Keywords** Thermal stability · 1,3-Dimethylimidazolium nitrate · Reaction mechanism · Decomposition mechanism function · Runaway reaction

## List of symbols

$A$	Pre-exponential factor (min <sup>-1</sup> )
$E_a$	Apparent activation energy (kJ mol <sup>-1</sup> )
$h$	Planck constant (J s)
$k$	Reaction rate constant (min <sup>-1</sup> )
$k_B$	Boltzmann constant (J K <sup>-1</sup> )
$n$	Reaction order
$P_{\max}$	Maximum pressure (psig)
$R$	Molar gas constant (J mol <sup>-1</sup> K <sup>-1</sup> )
$r$	Linear correlation coefficient
$T$	Reaction temperature (K)
$T_{\text{end}}$	Termination temperature of decomposition (°C)
$T_{\max}$	Maximum temperature (°C)
$\text{TMR}_{\text{ad}}$	Time to maximum rate under adiabatic condition (h)
$T_{\text{NR}}$	No return temperature (°C)

$T_{\text{onset}}$	Onset temperature of decomposition (°C)
$T_p$	Peak temperature of decomposition (°C)
$T_{\text{start}}$	Start temperature of decomposition (°C)
$\Delta G^\ddagger$	Gibbs free energy (kJ mol <sup>-1</sup> )
$\Delta H^\ddagger$	Enthalpy (kJ mol <sup>-1</sup> )
$\Delta S^\ddagger$	Entropy (J mol K <sup>-1</sup> )
$\Delta P_{\text{ad}}$	Adiabatic pressure rise (psig)
$\Delta T_{\text{ad}}$	Adiabatic temperature rise (°C)
$\alpha$	Degree of conversion
$\beta$	Heating rates (°C min <sup>-1</sup> )
$\Phi$	Thermal inertia

## Introduction

Ionic liquids (ILs) are known as room-temperature molten salts with melting points below 100.0 °C, and they combine organic cations with organic or inorganic anions. ILs have numerous attractive properties, such as extremely low vapor pressure, low melting point, wide liquid range, good thermal stability, and wide electrochemical windows [1]. Based on their excellent performance, ILs are widely used as organic solvents [2–4], catalysts [5] and heat transfer

✉ Shang-Hao Liu  
shliu998@163.com

<sup>1</sup> School of Chemical Engineering, Anhui University of Science and Technology, Huainan 232001, Anhui, China

<sup>2</sup> Department of Fire Science, Wu Feng University, 117 Jianguo Rd., Sec.2, Minsyong, Chiayi 62153, Taiwan, ROC

fluids [6–8] for separations [9] as well as electrochemistry [10–13].

However, according to US Occupational Safety and Health Administration (OSHA) regulations, ILs are classified as IIIB combustible materials, which means that ILs are not sufficiently safe when near fire or heat sources [14, 15]. This classification implies that ILs will decompose under high ambient temperatures. On the other hand, in the presence of nitrate, ILs can be used as energetic materials due to the high energy of the functional groups. Unfortunately, ILs may also lead to explosions and other serious safety problems if the cooling system fails or operates at incorrect process temperatures [16–18]. In the previous studies, there are few reports of thermal hazard for imidazolium nitrate ionic liquids [19]. Hence, it is critical to investigate the thermal stability and potential hazards for imidazolium nitrate ionic liquids during the applications.

We developed a methodology to estimate the thermal stability and thermal hazard of 1,3-dimethylimidazolium nitrate ([Mmim]NO<sub>3</sub>) using thermogravimetry (TG) and vent sizing package 2 (VSP2). The specific targets of this research were as follows:

- To reveal the short-term thermal stability of [Mmim]NO<sub>3</sub> by TG experiment, which uses a non-isothermal medium;
- To establish the reaction mechanism of [Mmim]NO<sub>3</sub> using the data from the TG curves;
- To calculate thermokinetic parameters such as the apparent activation energy ( $E_a$ ) and the pre-exponential factor ( $A$ ) of [Mmim]NO<sub>3</sub> by Flynn–Wall–Ozawa (F–W–O), Kissinger–Akahira–Sunose (K–A–S) and Starink methods;
- To estimate the related parameters of process safety during a thermal runaway reaction using VSP2 under adiabatic conditions.

## Experimental and methods

### Samples

Ninety-eight mass% [Mmim]NO<sub>3</sub> in the solid state was received from Hua Wei Rui Ke Chemical Co., Beijing, China. Experimental techniques using dynamic and adiabatic approaches were proposed in this study. According to the experimental techniques, we could determine the thermal stability and runaway reaction of [Mmim]NO<sub>3</sub>.

### Thermogravimetry (TG)

SDT Q600 from TA Instruments, Inc. (Delaware, USA) was used to perform the TG experiment. [Mmim]NO<sub>3</sub>

sample in the range of 6.0–8.0 mg each was placed in an open alumina crucible. The scanning TG experiments were performed in a nitrogen atmosphere, with the gas purging at a flow rate of 100.0 mL min<sup>-1</sup>. Dynamic experiments were performed at a temperature range from 25.0 to 400.0 °C, with heating rates of 2.0, 4.0, 6.0, 8.0 and 10.0 °C min<sup>-1</sup>. TG curves have been further applied to obtain the corresponding thermokinetic parameters and the most likely thermokinetic model functions using mathematical approaches.

### Vent sizing package 2

VSP2 from Fauske & Associates, Inc. (Illinois, USA) was applied to measure the adiabatic state that can simulate the reactor in the process. It uses the heat–wait–search mode, which can furnish temperature and pressure traces versus time from the dynamic scanning test in the test cell (112.0 mL), which is suitable for solid samples due to the low thermal inertia ( $\phi$ ) of approximately 1.05–1.20. In this study, approximately 3.0 g of [Mmim]NO<sub>3</sub> was loaded into the test cell.

### Thermal analysis theory

The thermal decomposition of [Mmim]NO<sub>3</sub> complies with the following rate Eq. 1:

$$\frac{d\alpha}{dt} = k(T) \cdot f(\alpha) \quad (1)$$

where  $d\alpha/dt$  is the conversion rate of different times,  $k(T)$  is the Arrhenius rate constant, and  $f(\alpha)$  is the differential mechanism function.

According to the Arrhenius equation,  $k(T)$  can be defined as:

$$k(T) = A \cdot \exp\left(-\frac{E_a}{RT}\right) \quad (2)$$

where  $A$  is the pre-exponential factor,  $R$  is the molar gas constant (8.314 J mol<sup>-1</sup> K<sup>-1</sup>), and  $E_a$  is the apparent activation energy.

$\alpha$  is the degree of conversion as follows:

$$\alpha = \frac{W_i - W_t}{W_i} \quad (3)$$

where  $W_i$  is the initial mass and  $W_t$  represents the mass of the sample at time  $t$ .

Considering the constant heating rate  $\beta$  in the non-isothermal heating mode, Eq. 1 is rearranged to the following form [20]:

$$\frac{d\alpha}{dT} = \frac{A}{\beta} \times \exp\left(-\frac{E_a}{RT}\right) \times f(\alpha) \quad (4)$$

Equation 4 is the basis of the isoconversational mode. In this study, we selected F–W–O, K–A–S, and Starink methods to investigate the thermokinetic parameters.

(a) F–W–O method

The F–W–O method is a typical isoconversational mode. It uses multiple heating rate curves to determine the thermokinetic parameters. The equation is expressed as [13]:

$$\lg(\beta) = \lg \left[ \frac{AE_a}{RG(\alpha)} \right] - 2.315 - 0.4567 \frac{E_a}{RT} \quad (5)$$

where  $G(\alpha)$  is the integral mechanism function.  $G(\alpha)$  is a stationary constant when  $\alpha$  is certain.  $E_a$  can be obtained from the straight line by plotting  $\lg(\beta)$  versus  $1/T$ .

(b) K–A–S method

The K–A–S method is also based on the isoconversational mode, which is applied as a model-free approach. The equation is as follows [21]:

$$\ln \frac{\beta}{T^2} = \ln \left[ \frac{AR}{G(\alpha)E_a} \right] - \frac{E_a}{RT} \quad (6)$$

A straight line can be obtained by plotting  $\ln(\beta/T^2)$  versus  $1/T$ , which can be applied to solve the thermokinetic parameter  $E_a$ .

The pre-exponential factor  $A$  can be calculated based on the K–A–S method by the following equation:

$$A = \frac{\beta E_a}{RT_p^2} \exp \left( \frac{E_a}{RT_p} \right) \quad (7)$$

where  $T_p$  is the peak temperature of DTG.

(c) Starink method

Starink summarized the Kissinger, Ozawa, and Boswell methods and then further refined the temperature integral. The revised mathematical equation is expressed as Eq. 8 [22]:

$$\ln \frac{\beta}{T^{1.8}} = C_s - \frac{E_a}{RT} \quad (8)$$

The plot of  $\ln(\beta/T^{1.8})$  versus  $1/T$  forms a straight line, and  $E_a$  would be obtained from the slope. On the whole,  $E_a$  can be received from Eqs. 4–8, which do not consider the differential mechanism function  $g(\alpha)$  and the integral mechanism function  $G(\alpha)$ .

## Results and discussion

### Short-term thermal stability

The thermal stability of [Mmim]NO<sub>3</sub> was investigated by TG experiments. The TG–DTG data of [Mmim]NO<sub>3</sub> were obtained by the non-isothermal method under a nitrogen atmosphere, as shown in Fig. 1.

Figure 1a shows three mass loss steps in the TG curve, which were defined as steps I, II and III. The temperature of the mass loss in step I was at approximately 100.0 °C, which may be caused by evaporation of water existing in [Mmim]NO<sub>3</sub>. For this step, the mass losses were 2.0, 1.0, 1.7, 1.1, and 1.5% at the heating rates of 2.0, 4.0, 6.0, 8.0, and 10.0 °C min<sup>−1</sup>, respectively. Step II was the main stage of mass loss, which was caused by the thermal decomposition of [Mmim]NO<sub>3</sub>. The peak temperature ( $T_p$ ) of [Mmim]NO<sub>3</sub> was around 179.0–202.0 °C at five heating rate. Figure 1b illustrates that  $T_p$  increases with increasing

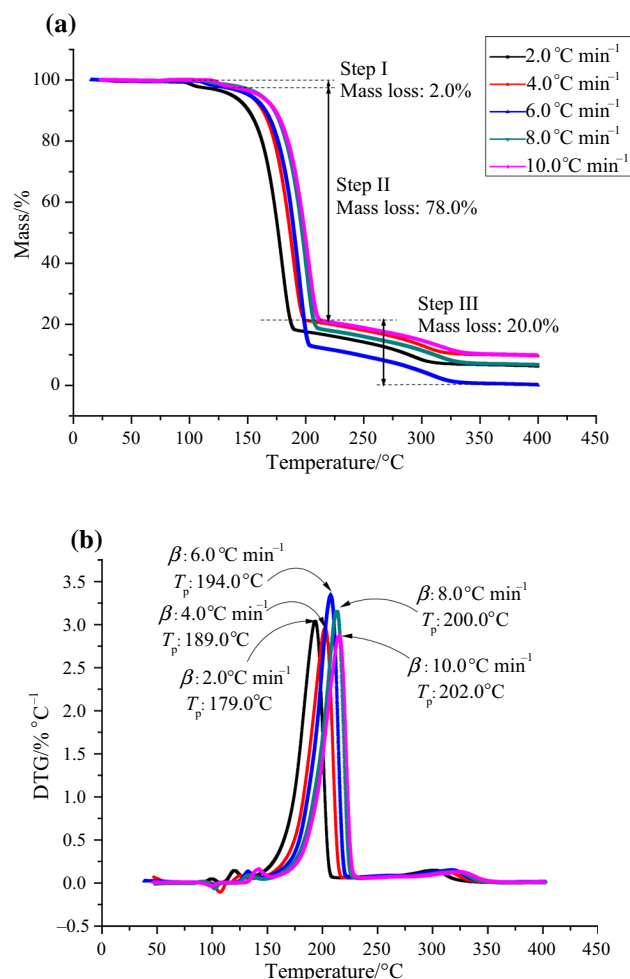


**Fig. 1** a TG curve and b DTG curves for the decomposition of [Mmim]NO<sub>3</sub> at five heating rates

**Table 1** Non-isothermal data for the thermal decomposition of [Mmim]NO<sub>3</sub> at five heating rates

$\beta/^\circ\text{C min}^{-1}$	$T_{\text{start}}/^\circ\text{C}$	$T_{\text{onset}}/^\circ\text{C}$	$T_{\text{p}}/^\circ\text{C}$	$T_{\text{end}}/^\circ\text{C}$	$T_{0.10}/^\circ\text{C}$
2	116	161	179	336	151
4	122	168	189	345	163
6	127	174	194	349	166
8	133	179	200	352	172
10	135	182	202	354	174

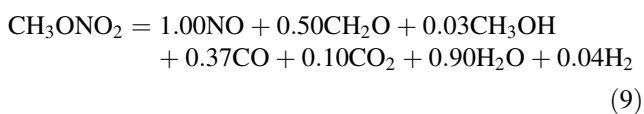
$T_{\text{p}}$  and  $T_{0.10}$  are the temperatures for the DTG peak and 10% degree of conversion, respectively

heating rate; however, the temperature variation range was narrow. The start temperature ( $T_{\text{start}}$ ) and onset temperature ( $T_{\text{onset}}$ ) of thermal decomposition under five heating rates are listed in Table 1.

$T_{\text{onset}}$  is applied to represent the short-term thermal stability of ILs. It can be seen that the  $T_{\text{onset}}$  of [Mmim]NO<sub>3</sub> was less than 200.0 °C. The effect of heating rate on  $T_{\text{onset}}$  is not obvious for [Mmim]NO<sub>3</sub>.  $T_{\text{start}}$  is lower than  $T_{\text{onset}}$ , at approximately 45.0–47.0 °C. This result indicates that  $T_{\text{onset}}$  is higher than the actual decomposition temperature. The temperature for a 10% conversion rate ( $T_{0.10}$ ) was 151.0–174.0 °C which was measured under non-isothermal conditions at different heating rates. In previous studies,  $T_{\text{onset}}$ ,  $T_{\text{start}}$ , and  $T_{0.10}$  were used to evaluate the thermal stability of ILs via TG. For example, the  $T_{\text{onset}}$  of 1-butyl-3-methylimidazolium chloride ([Bmim]Cl) is approximately 234.0–270.0 °C [23–27], and that of 1-butyl-3-methylimidazolium tetrafluoroborate ([Bmim]BF<sub>4</sub>) is approximately 315.0–424.0 °C [23–25, 28]. The results of [Mmim]NO<sub>3</sub> can be considered as a manifestation of lower thermal stability than other imidazolium ILs.

## Decomposition mechanism

Step II is the main decomposition stage that will produce a variety of decomposition products, including methyl nitrate (CH<sub>3</sub>ONO<sub>2</sub>), which is formed by the reaction of the nitrate anion with a methyl group that was produced during the breakdown of [Mmim]NO<sub>3</sub>. Step III (Fig. 1a) is obviously different from step II in that the rate of mass loss is significantly reduced. Obviously, the decomposition mode of step III is altered. The decomposition temperature range of step III is 190.0–332.0 °C, and CH<sub>3</sub>ONO<sub>2</sub> produced by step II will decompose in this temperature range. The reaction equation can be expressed as follows [29, 30]:



Therefore, the mass loss of step III can be interpreted as the decomposition of CH<sub>3</sub>ONO<sub>2</sub>.

## Decomposition thermokinetics

To obtain the thermokinetic parameters of [Mmim]NO<sub>3</sub> such as  $E_{\text{a}}$  and  $A$ , the TG curves at heating rates of 2.0, 4.0, 6.0, 8.0 and 10.0 °C min<sup>-1</sup> were addressed by mathematical means, and three isoconversional methods (Eqs. 5–8) were employed. The results are shown in Figs. 2–4. Excellent linear relationships were observed under different heating rates with the three methods.

Table 2 shows the thermokinetic parameters obtained by the different methods. The  $E_{\text{a}}$  values were 121.2, 119.8, and 121.9 kJ mol<sup>-1</sup> obtained by the F–W–O, Starink, and K–A–S methods, respectively. Overall, the  $E_{\text{a}}$  values calculated by the three methods were similar. The average  $E_{\text{a}}$  value of the three methods was 121.0 kJ mol<sup>-1</sup>, and the linear correlation coefficient ( $r$ ) was 0.9938, with a good

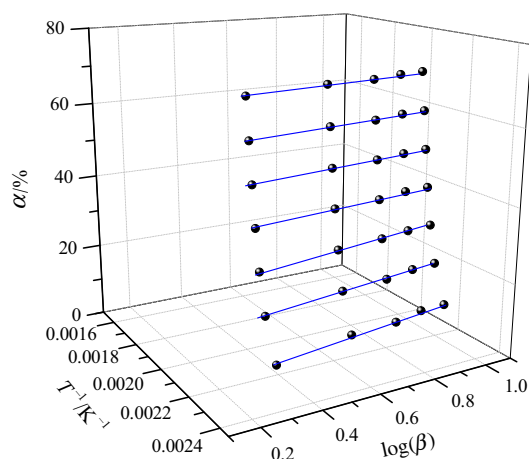


**Fig. 2** Linear curves of  $\lg(\beta)$  versus  $1/T$  by the F–W–O method

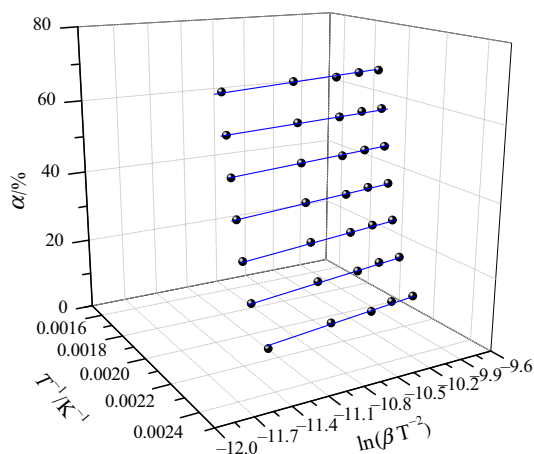


**Fig. 3** Linear curves of  $\ln(\beta/T^2)$  versus  $1/T$  by the K–A–S method

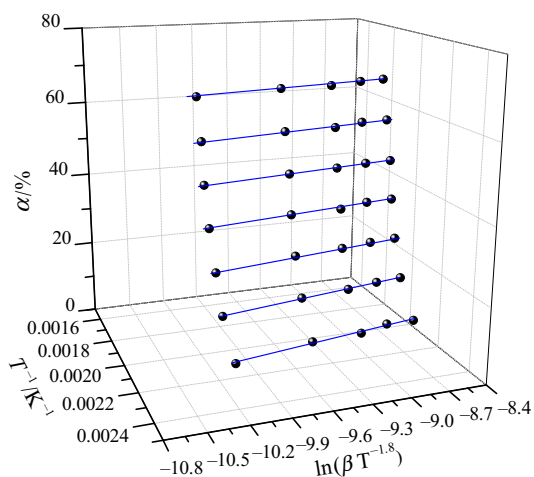


**Fig. 4** Linear curves of  $\ln(\beta/T^{1.8})$  versus  $1/T$  by the Starink method

**Table 2** Kinetic parameters obtained by F–W–O, Starink and K–A–S methods of  $[\text{Mmim}]\text{NO}_3$

Method	$E_a/\text{kJ mol}^{-1}$	$A/\text{min}^{-1}$	$r$
F–W–O method	121.2	–	0.9850
Starink method	119.8	–	0.9823
K–A–S method	121.9	$3.6 \times 10^{12}$	0.9837

**Table 3** Kinetic parameters obtained of  $[\text{Mmim}]\text{NO}_3$  by Šatava–Šesták method at different kinetic models

Model	$E_a/\text{kJ mol}^{-1}$	$A/\text{min}^{-1}$	$r$
$A_1$	123.1	$2.7 \times 10^{12}$	0.9901
$A_{1.5}$	75.4	$4.2 \times 10^6$	0.9821
$R_1$	95.9	$8.5 \times 10^8$	0.9885
$R_{1/4}$	101.7	$7.4 \times 10^{10}$	0.9921
$R_{1/2}$	92.1	$2.5 \times 10^{10}$	0.9899
$P_{7/10}$	122.1	$6.5 \times 10^{12}$	0.9893

$$A_1: G(\alpha) = -\ln(1 - \alpha)$$

$$A_{1.5}: G(\alpha) = [-\ln(1 - \alpha)]^{2/3}$$

$$R_1: G(\alpha) = \alpha$$

$$R_{1/4}: G(\alpha) = 1 - (1 - \alpha)^{1/4}$$

$$R_{1/2}: G(\alpha) = 1 - (1 - \alpha)^{1/2}$$

$$P_{7/10}: G(\alpha) = \alpha^{10/7}$$

correlation. According to Eq. 7 and the  $E_a$  calculated by the K–A–S method, the determined  $\lg A$  was  $12.5 \text{ min}^{-1}$ .

As for the thermal decomposition mechanism selection for the main reaction stage, the following four conditions must be observed: (a)  $E_a$  selected must fit within the range of the thermal decomposition kinetic parameters ( $E_a = 80.0\text{--}250.0 \text{ kJ mol}^{-1}$ ); (b)  $r$  is greater than 0.98; (c)  $E_a$  and  $\lg A$  obtained from the integral and differential methods

are roughly the same; and (d) the mechanism function selected must be in agreement with the tested sample state [31, 32]. The results using Šatava–Šesták (Eq. 10) at different kinetic models are listed in Table 3.

$$\lg G(\alpha) = \lg \frac{AE_a}{\beta R} - 2.315 - 0.4567 \frac{E_a}{RT} \quad (10)$$

Obviously, the values of  $E_a$  ( $123.1 \text{ kJ mol}^{-1}$ ) and  $A$  ( $2.7 \times 10^{12} \text{ min}^{-1}$ ) calculated by the integral method (Šatava–Šesták method) under the nucleation and growth decomposition mechanism  $A_1$  were almost the same that calculated by the differential method (F–W–O method). Meanwhile, the  $E_a$  ( $122.1 \text{ kJ mol}^{-1}$ ) and  $A$  ( $6.5 \times 10^{12} \text{ min}^{-1}$ ) calculated under the power law decomposition mechanism  $P_{7/10}$  as well as closed to the values using F–W–O method. However,  $P_{7/10}$  belongs to accelerating models, which represent processes whose rate increases continuously with increasing the extent of conversion and reaches its maximum at the end of the process. Apparently, the accelerating model was not fit for the sample of  $[\text{Mmim}]\text{NO}_3$  according to the TG curves. Therefore, the decomposition mechanism  $A_1$  was more suitable for the decomposition of  $[\text{Mmim}]\text{NO}_3$  considering the actual situation. The mechanism function is Avramo–Erofeev equation with  $n = 1$ ,  $G(\alpha) = -\ln(1 - \alpha)$  and  $f(\alpha) = 1 - \alpha$ . Substituting  $E_a$  with  $123.1 \text{ kJ mol}^{-1}$  and  $A$  with  $2.7 \times 10^{12} \text{ min}^{-1}$  into Eq. 1, the kinetic equation of the main reaction stage may be described as:

$$\frac{d\alpha}{dt} = 10^{10.65} \times (1 - \alpha) \times \exp\left(\frac{-1.48 \times 10^4}{T}\right) \quad (11)$$

Considering the effect of constant heating rate  $\beta$ , Eq. 11 is rearranged to the following form:

$$\frac{d\alpha}{dt} = \frac{10^{10.65}}{\beta} \times (1 - \alpha) \times \exp\left(\frac{-1.48 \times 10^4}{T}\right) \quad (12)$$

The entropy of activation ( $\Delta S^\ddagger$ ), enthalpy of activation ( $\Delta H^\ddagger$ ), and free energy of activation ( $\Delta G^\ddagger$ ) for  $[\text{Mmim}]\text{NO}_3$  as resolved by Eqs. 13–15 were  $68.1 \text{ J mol K}^{-1}$ ,  $118.1$  and  $86.6 \text{ kJ mol}^{-1}$ , respectively, which can be used to supplementary characterize the thermal decomposition reaction.

$$A = \frac{k_B T_p}{h} \exp\left(\frac{\Delta S^\ddagger}{R}\right) \quad (13)$$

$$\Delta H^\ddagger = E_a - RT_p \quad (14)$$

$$\Delta G^\ddagger = \Delta H^\ddagger - T_p \Delta S^\ddagger \quad (15)$$

where the values of  $A$  and  $E_a$  are calculated by the K–A–S method,  $T_p$  is peak temperature,  $k_B$  is the Boltzmann constant ( $1.3807 \times 10^{-27} \text{ J K}^{-1}$ ), and  $h$  is the Planck constant ( $6.626 \times 10^{-34} \text{ J s}$ ).



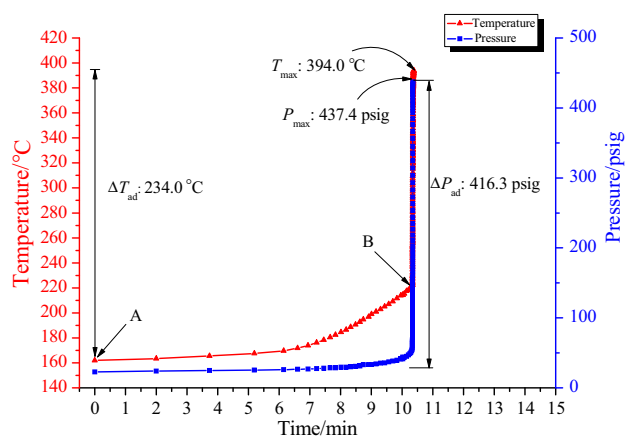


**Fig. 5** Pressure and temperature versus time for the thermal decomposition of [Mmim]NO<sub>3</sub> by VSP2

### Thermal hazard analysis by VSP2

In this research stage, under an adiabatic environment, the thermokinetic parameters of process safety for [Mmim]NO<sub>3</sub> were estimated by VSP2. The determined onset temperature  $T_{\text{onset}}$  was 162.0 °C. As obtained by VSP2, the maximum temperature ( $T_{\text{max}}$ ), the maximum pressure ( $P_{\text{max}}$ ), the maximum temperature rise rate ( $(dT/dt)_{\text{max}}$ ), and the maximum pressure rise rate ( $(dP/dt)_{\text{max}}$ ) were 394.0 °C, 437.4 psig, 39,828.0 °C min<sup>-1</sup>, and 73,331.0 psig min<sup>-1</sup>, respectively.

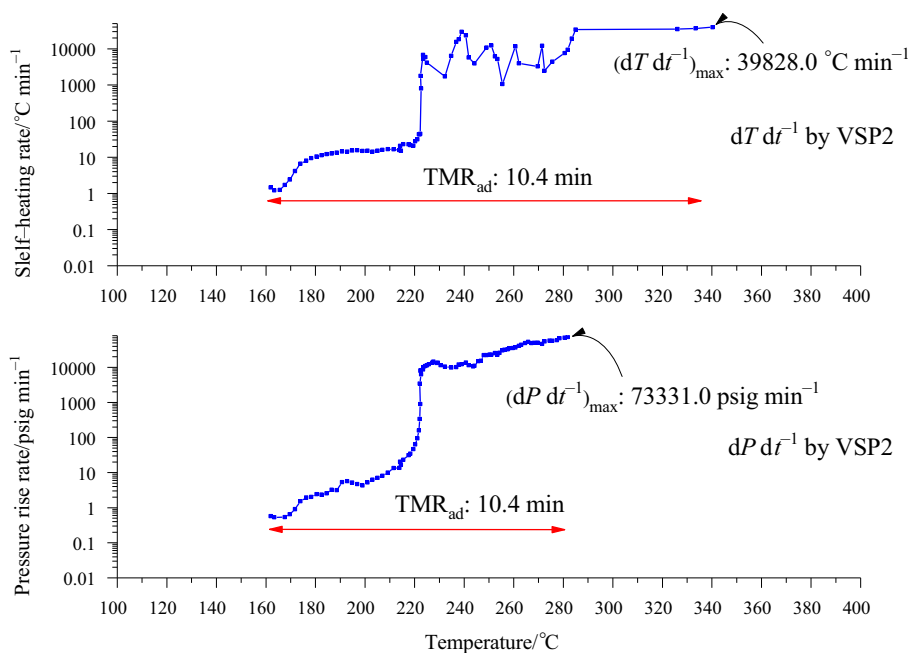
Figure 5 illustrates the curves of pressure and temperature versus time during the exothermic behavior of [Mmim]NO<sub>3</sub>. Point A was the reaction start time, and when the reaction reached point B, the reaction rate increased

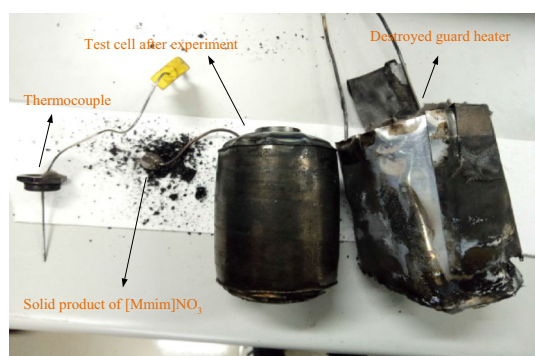
dramatically, and the system reached the no-return temperature ( $T_{\text{NR}}$ ), which means the maximum heat release rate and the maximum temperature are reached within a very short time. The observed adiabatic temperature rise ( $\Delta T_{\text{ad}}$ ) and adiabatic pressure rise ( $\Delta P_{\text{ad}}$ ) were 234.0 °C and 416.3 psig, respectively.

Figure 6 indicates the curves of self-heating rate and pressure rise rate versus the runaway reaction temperature of [Mmim]NO<sub>3</sub> under adiabatic conditions. When the temperature reached  $T_{\text{NR}}$ , the pressure rise rate increased rapidly, and  $(dP/dt)_{\text{max}}$  reached 73,331.0 psig min<sup>-1</sup>. Obviously, the exothermic behavior of [Mmim]NO<sub>3</sub> was from the standpoint that  $(dT/dt)_{\text{max}}$  and  $(dP/dt)_{\text{max}}$  increased in a short time of 10.4 min, from onset to apex.

According to Semenov theory [33], runaway reactions will occur if the temperature rises sharply to a no-return temperature when the heat generation rate is greater than the heat removal rate. The critical runaway temperature and unstable reaction criteria might lead to a fire, explosion, or chemical release. In the process of this adiabatic experiment, the system cannot effectively remove the heat generated, eventually causing the destruction of the test cell by a runaway reaction, which is shown in Fig. 7. The results showed that a rapid runaway reaction existed in [Mmim]NO<sub>3</sub>. This means [Mmim]NO<sub>3</sub> has the potential for thermal runaway phenomena if the cooling system fails in the process.

**Fig. 6** Self-heating rate and pressure rise rate versus temperature of [Mmim]NO<sub>3</sub> by VSP2





**Fig. 7** VSP2 test cell damaged by runaway reaction under adiabatic conditions

## Conclusions

The short-term thermal stability and decomposition kinetics of [Mmim]NO<sub>3</sub> were investigated using non-isothermal TG under a nitrogen atmosphere. The results showed three mass loss stages. Step I was the water evaporation, step II was caused by the decomposition of [Mmim]NO<sub>3</sub>, and step III was the decomposition of methyl nitrate, which was a decomposition product of [Mmim]NO<sub>3</sub> in step II. The maximum onset temperature was 182.0 °C when the heating rate was 10.0 °C min<sup>-1</sup>. The  $E_a$  value was 119.0–124.0 kJ mol<sup>-1</sup> as obtained from different methods. The main exothermic decomposition reaction mechanism of [Mmim]NO<sub>3</sub> was the nucleation and growth with  $n = 1.0$ . The kinetic equation can be expressed as:

$$\frac{dx}{dt} = \frac{10^{10.65}}{\beta} \times (1 - \alpha) \times \exp\left(\frac{-1.48 \times 10^4}{T}\right).$$

As for the thermal hazard analysis of [Mmim]NO<sub>3</sub> under adiabatic conditions by VSP2, the maximum self-heating rate and pressure rise rate were 39,828.0 °C min<sup>-1</sup> and 73,331.0 psig min<sup>-1</sup>, respectively. These results indicated that [Mmim]NO<sub>3</sub> has potential thermal runaway hazards. Therefore, all of the thermal hazard information that was gained in this research can be provided to the relevant factory for decreasing casualties.

**Acknowledgements** The authors would like to express their appreciation to the Anhui Province Education Department Natural Sciences Key Fund, China, under the Contract Number KJ2017A078, as well as the donors of the Anhui University of Science and Technology, China, under the Contract Number QN201613 for financial support of this study.

## References

- Sheldon RA. Fundamentals of green chemistry: efficiency in reaction design. *Chem Soc Rev.* 2012;41:1437–51.
- Quraishi KS, Bustam QM, Krishnan S, Khan MI, Wilfred CD, Leveque JM. Thermokinetics of alkyl methylpyrrolidinium [NTf<sub>2</sub>] ionic liquids. *J Therm Anal Calorim.* 2017;129:261–70.
- Wang HY, Jia YZ, Wang XH, Yao Y, Jing Y. Physical–chemical properties of nickel analogs ionic liquid based on choline chloride. *J Therm Anal Calorim.* 2014;115:1779–85.
- Usula M, Plechkova NV, Piras A, Porcedda S. Ethylammonium alkanoate-based ionic liquid + water mixtures. *J Therm Anal Calorim.* 2015;121:1129–37.
- Ren YL, Wang BY, Tian XZ, Zhao S, Wang JJ. Aerobic oxidative bromination of arenes using an ionic liquid as both the catalyst and the solvent. *Tetrahedron Lett.* 2015;56:6452–5.
- Gharagheizi F, Sattari M, Ilani-Kashkouli P, Mohammadi AH, Ramjugernath D, Richon D. Quantitative structure–property relationship for thermal decomposition temperature of ionic liquids. *Chem Eng Sci.* 2012;84:557–63.
- Maton C, De VN, Stevens CV. Ionic liquid thermal stabilities: decomposition mechanisms and analysis tools. *Chem Soc Rev.* 2013;42:5963–77.
- Parajó JJ, Teijeira T, Fernández J, Salgado J, Villanueva M. Thermal stability of some imidazolium [NTf<sub>2</sub>] ionic liquids: isothermal and dynamic kinetic study through thermogravimetric procedures. *J Chem Eng.* 2017;112:105–13.
- Souza RL, Ventura SPM, Soares CMF, Coutinho JAP, Lima AS. Lipase purification using ionic liquids as adjuvants in aqueous two-phase systems. *Green Chem.* 2015;17:3026–34.
- Zhang ZH, Cui T, Zhang JL, Xiong H, Li GP, Sun LX, Xu F, Cao Z, Li F, Zhao JJ. Thermodynamic investigation of room temperature ionic liquid. *J Therm Anal Calorim.* 2010;101:1143–8.
- Keshavarz MH, Esmailpour K, Saani MH, Taghizadeh H. A new method for assessment of glass transition temperature of ionic liquids from structure of their cations and anions without using any computer codes. *J Therm Anal Calorim.* 2017;1:1–19.
- Zhao YS, Zhen YP, Jelle BP, Bostrom T. Measurements of ionic liquids thermal conductivity and thermal diffusivity. *J Therm Anal Calorim.* 2017;128:279–88.
- Sharma VK, Kataria J, Bhagour S. Thermodynamic investigations of 1-ethyl-3-methylimidazolium tetrafluoroborate and cycloalkane mixtures. *J Therm Anal Calorim.* 2014;118:431–47.
- Smiglak M, Reichert WM, Holbrey JD, Wilkes JS, Sun LY, Thrasher JS, Kirichenko K, Singh S, Katritzky AR, Rogers RD. Combustible ionic liquids by design: is laboratory safety another ionic liquid myth? *Chem Commun.* 2006;24:2554–6.
- Cao YY, Mu TC. Comprehensive investigation on the thermal stability of 66 ionic liquids by thermogravimetric analysis. *Ind Eng Chem Res.* 2014;53:8651–64.
- Wellens S, Thijs B, Binnemans K. How safe are protic ionic liquids? Explosion of pyrrolidinium nitrate. *Green Chem.* 2013;15:3484–5.
- Anouti M, Cailloncaravanier M, Floch CL, Lemordant D. Alkylammonium-based protic ionic liquids. II ionic transport and heat-transfer properties: fragility and ionicity rule. *J Phys Chem B.* 2008;112:9412–6.
- Smiglak M, Hines CC, Reichert WM, Vincek AS, Katritzky AR, Thrasher JS, Sun LY, McCrary PD, Beasley PA, Kelley SP, Rogers RD. Synthesis, limitations, and thermal properties of energetically-substituted, protonated imidazolium picrate and nitrate salts and further comparison with their methylated analogs. *New J Chem.* 2012;36:702–22.
- Diallo AO, Fayet G, Len C, Marlair G. Evaluation of heats of combustion of ionic liquids through use of existing and purpose-built models. *Ind Eng Chem Res.* 2012;51:3149–56.
- Grigante M, Brighenti M, Antolini D. Analysis of the impact of TG data sets on activation energy ( $E_a$ ). *J Therm Anal Calorim.* 2017;129:553–65.

21. Kissinger HE. Reaction kinetics in differential thermal analysis. *Anal Chem.* 1957;29:1702–6.
22. Starink MJ. A new method for the derivation of activation energies from experiments performed at constant heating rate. *Thermochim Acta.* 1996;288:97–104.
23. Fredlake CP, Crosthwaite JM, Hert DG, Aki SNVK, Brennecke JF. Thermophysical properties of imidazolium-based ionic liquids. *J Chem Eng.* 2004;49:954–64.
24. Wendler F, Todi LN, Meister F. Thermostability of imidazolium ionic liquids as direct solvents for cellulose. *Thermochim Acta.* 2012;528:76–84.
25. Huddleston JG, Visser AE, Reichert WM, Willauer HD, Broker GA, Rogers RD. Characterization and comparison of hydrophilic and hydrophobic room temperature ionic liquids incorporating the imidazolium cation. *Green Chem.* 2001;3:241–72.
26. Awad WH, Gilman JW, Nyden M, Harris RH, Sutto TE, Callahan J, Trulove PC, De Long HC, Fox DM. Thermal degradation studies of alkyl-imidazolium salts and their application in nanocomposites. *Thermochim Acta.* 2004;409:3–11.
27. Arellano IHJ, Guarino JG, Paredes FU, Arco SD. Thermal stability and moisture uptake of 1-alkyl-3-methylimidazolium bromide. *J Therm Anal Calorim.* 2011;103:725–30.
28. Valkenburg MEV, Vaughn RL, Williams M, Wilkes JS. Thermochemistry of ionic liquid heat-transfer fluids. *Thermochim Acta.* 2005;425:181–8.
29. Gray P, Griffiths JF, Hasegawa K. Nonisothermal decomposition of methyl nitrate: anomalous reaction order and activation energies and their correction. *Int J Chem Kinet.* 1981;13:817–31.
30. Gray BP, Rogers GT. The explosion and decomposition of methyl nitrate in the gas phase. *Trans Faraday Soc.* 1954;50:28–36.
31. Vyazovkin S, Burnham AK, Criado JM, Pérez-Maqueda LA, Popescu C, Sbirrazzuoli N. ICTAC Kinetics Committee recommendations for performing kinetic computations on thermal analysis data. *Thermochim Acta.* 2011;520:1–19.
32. Yi JH, Zhao FQ, Gao HX, Xu SY, Wang MC, Hu RZ. Preparation, characterization, non-isothermal reaction kinetics, thermodynamic properties, and safety performances of high nitrogen compound: hydrazine 3-nitro-1,2, 4-triazol-5-one complex. *J Hazard Mater.* 2008;153:261–8.
33. Semenov NN. Some problems of chemical kinetics and reactivity, vol. 2. Oxford: Pergamon Press; 1959. p. 330.